Expanded View Figures

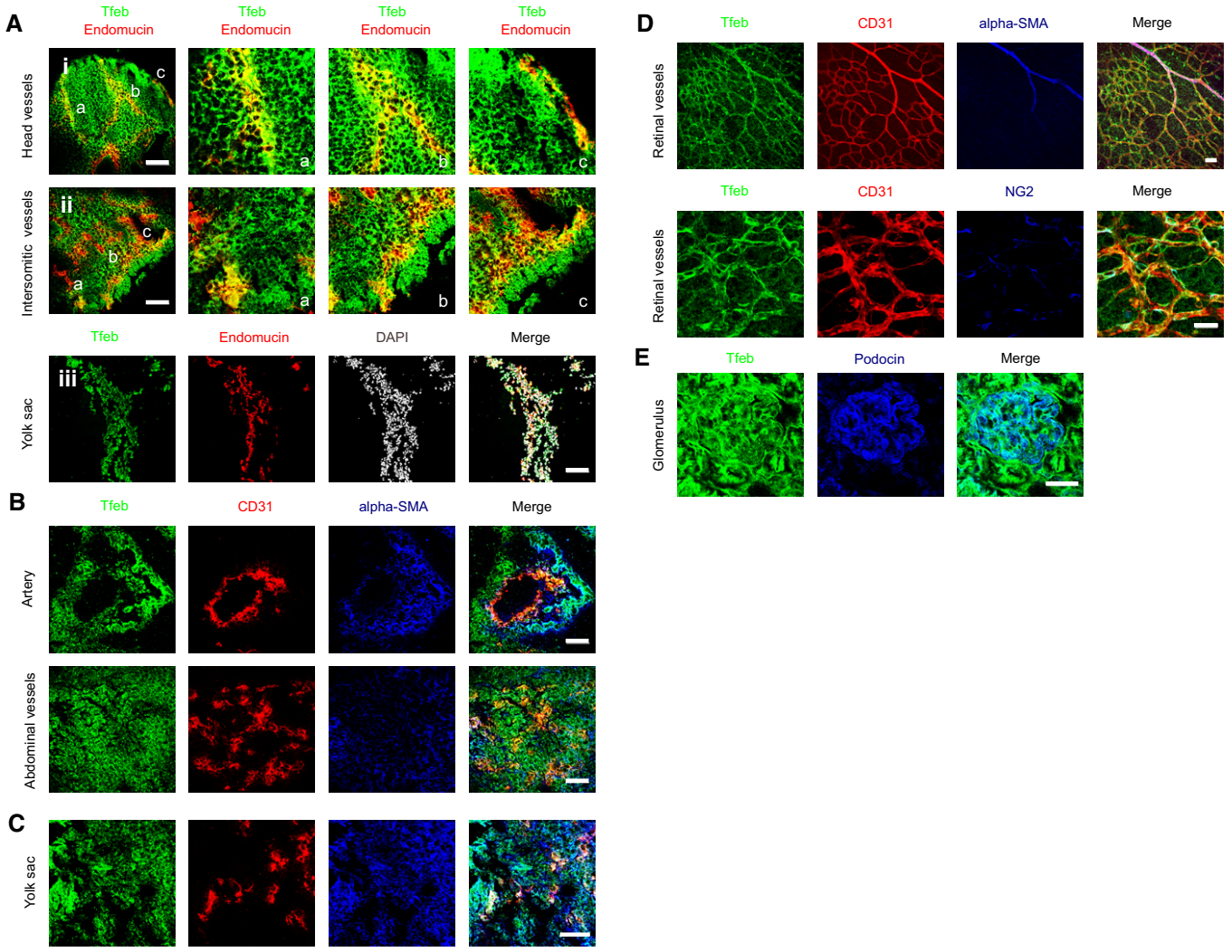

Figure EV1. Different cells types express Tfeb in embryos, yolk sac, retina, and kidney.

A *Tfeb* expression in embryos at E9.5 (embryos $n = 6$). Representative images of head (details a, b, c), intrasomitic region (details a, b, c), and yolk sac of *Tfeb-EGFP* embryos stained with anti-GFP and anti-endomucin Abs (scale bars: 100 μm).

B–E Tfeb expression in ECs and smooth muscle cells in embryos, retina, and kidney. Representative images of *Tfeb-EGFP* embryos (E9.5) (B), yolk sac (E9.5) (C), retina (p5) (D), and renal glomerulus (E) (embryos and mice $n = 6$) stained with anti-CD31, anti-alpha SMA, anti-NG2, anti-podocin, and anti-GFP Abs (scale bars: 100 μm).

Figure EV2. *Tfeb* deletion in embryos and pups.

A EC *Tfeb* deletion does not induce alterations in the embryonic vasculature at E9.5 (embryos $n = 6$). Representative images of whole-mount embryos (i) (scale bars: 0.5 mm). Vessels of the head (ii), ocular (iii), and intrasomitic regions (iv) were stained with anti-endomucin Ab (scale bars: 100 μm).

B EC *Tfeb* deletion induces embryonic hypoxia at E10.5 (embryos $n = 6$). Representative images of vessels and tissues of the head (i) and intrasomitic region (ii) of control and $Tfeb^{EC-/-}$ embryos stained with anti-endomucin (red) and the hypoxic marker pimonidazole (green; scale bars: 100 μm).

C Expression of Tie2 and markers of the endothelial and hematopoietic lineages in $Tfeb^{EC-/-}$ yolk sacs at E9.5. Bar graphs indicate the percentage of yolk sac $Tie2^+$ cells or Flk^+ or $CD31^+$ or $CD117^+/CD41^+$ and $CD117^+/CD71^+$ within the $Tie2^+$ population ($n = 3$, mean ± SEM; $^*P < 0.01$ versus control mice by Student's *t*-test).

D Genotype of $Tfeb^{iEC}$ mice. Schematic representation of murine *Tfeb*, the targeted allele and the knockout allele (delta allele), and qPCR analysis of mRNA encoded by *Tfeb* exon 5–6 in lung ECs and epithelial cells isolated from control, $Tfeb^{iEC-/+}$, and $Tfeb^{iEC-/-}$ mice. Data are expressed as relative fold-change compared with the expression in control mice after normalization to the housekeeping gene TBP (mice $n = 3$, mean ± SEM; $^*P < 0.01$ and $^{**}P < 0.001$ versus control mice by Student's *t*-test).

E Tfeb expression in renal tissue of control and $Tfeb^{iEC-/-}$ mice (p17). Representative images of renal glomerulus, artery, interstitial vessels, and the surrounding tissue of control and $Tfeb^{iEC-/-}$ mice (mice $n = 6$). Tissues were stained with anti-CD31 and anti-GFP Abs (scale bars: 100 μm).

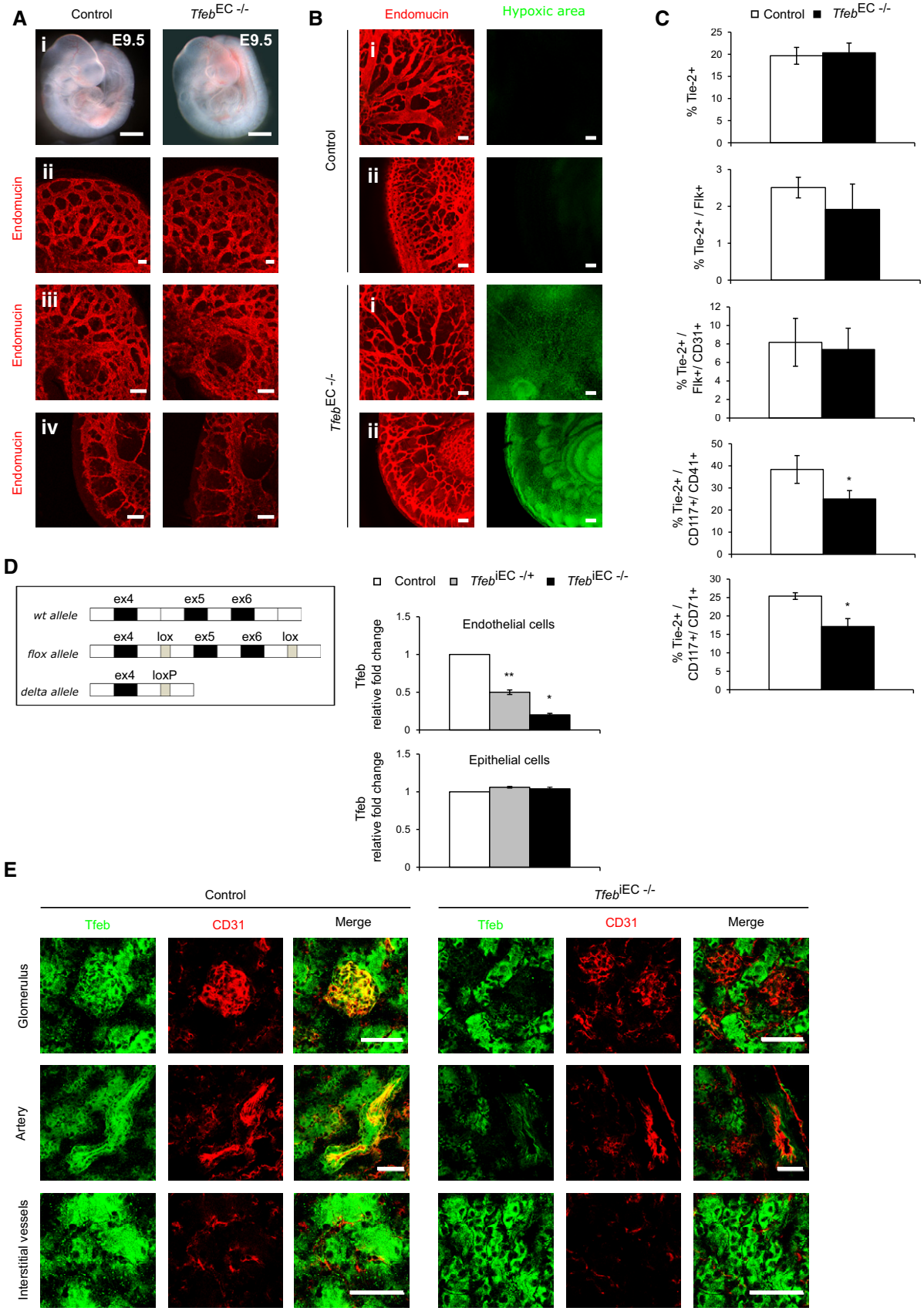
A
Control
Tfeb EC -/-
E9.5
E9.5
Endomucin
Endomucin
Endomucin
B
Endomucin
Hypoxic area
Control
Tfeb EC -/-
C
Control
Tfeb EC -/-
% Tie-2+
% Tie-2+ / Flk+
% Tie-2+ / Flk+/ CD31+
% Tie-2+ / CD117+/ CD41+
% Tie-2+ / CD117+/ CD71+
D
wt allele
flox allele
delta allele
ex4
ex5
ex6
lox
loxP
Control
Tfeb iEC -/+
Tfeb iEC -/-
Endothelial cells
Epithelial cells
Tfeb relative fold change
E
Control
Tfeb iEC -/-
Tfeb
CD31
Merge
Glomerulus
Artery
Interstitial vessels

Figure EV2.

Figure EV3. Post-natal maturation of retinal and renal vasculature after endothelium *Tfeb* silencing.

A EC *Tfeb* deletion compromises retinal vascular maturation at p10 and p15. Representative images of immunostaining of vascular front and vascular plexus of retina of control and $Tfeb^{iEC-/-}$ mice (p10, p15) with an anti-iB4 Ab (scale bars: 50 μm).

B–D EC *Tfeb* deletion compromises glomerular development and renal vascularization at p17. (B) Representative images of renal trichrome staining of control and $Tfeb^{iEC-/-}$ mice at p17 (original magnification x10, scale bars: 25 μm). (C) Bar graph indicates the $CD31^+$ vascular area in control and $Tfeb^{iEC-/-}$ mice (p17; mice $n = 5$, mean ± SEM; $^{**}P < 0.001$ versus control mice by Student's *t*-test). (D) EC *Tfeb* deletion compromises renal vascularization at p27. Bar graph indicates the $CD31^+$ vascular area in control and $Tfeb^{iEC-/-}$ mice (p27; mice $n = 5$, mean ± SEM; $^{**}P < 0.001$ versus control mice by Student's *t*-test).

E EC *Tfeb* deletion correlates with collagen deposition in kidney at p27. Representative images of immunostaining of kidney of control and $Tfeb^{iEC-/-}$ mice (p27) with anti-collagen I, anti-collagen V, and anti-collagen IV antibodies (scale bars: 50 μm). Quantification area per field (mean ± SEM): collagen I: 26,107.2 ± 3,200.82 μm^2 in control mice versus 43,069 ± 9,754.7 μm^2 in $Tfeb^{iEC-/-}$ mice, mice $n = 4$, $P = 0.02$ versus control mice by Student's *t*-test; collagen V: 33,500.4 ± 4,201 μm^2 in control mice versus 47,007.9 ± 6,287.7 μm^2 in $Tfeb^{iEC-/-}$ mice, mice $n = 4$, $P = 0.04$ versus control mice by Student's *t*-test; collagen IV: 10,972.12 ± 1,856.8 μm^2 in control mice versus 17,525.07 ± 2,106.58 μm^2 in $Tfeb^{iEC-/-}$ mice, mice $n = 4$, $P = 0.03$ versus control mice by Student's *t*-test)

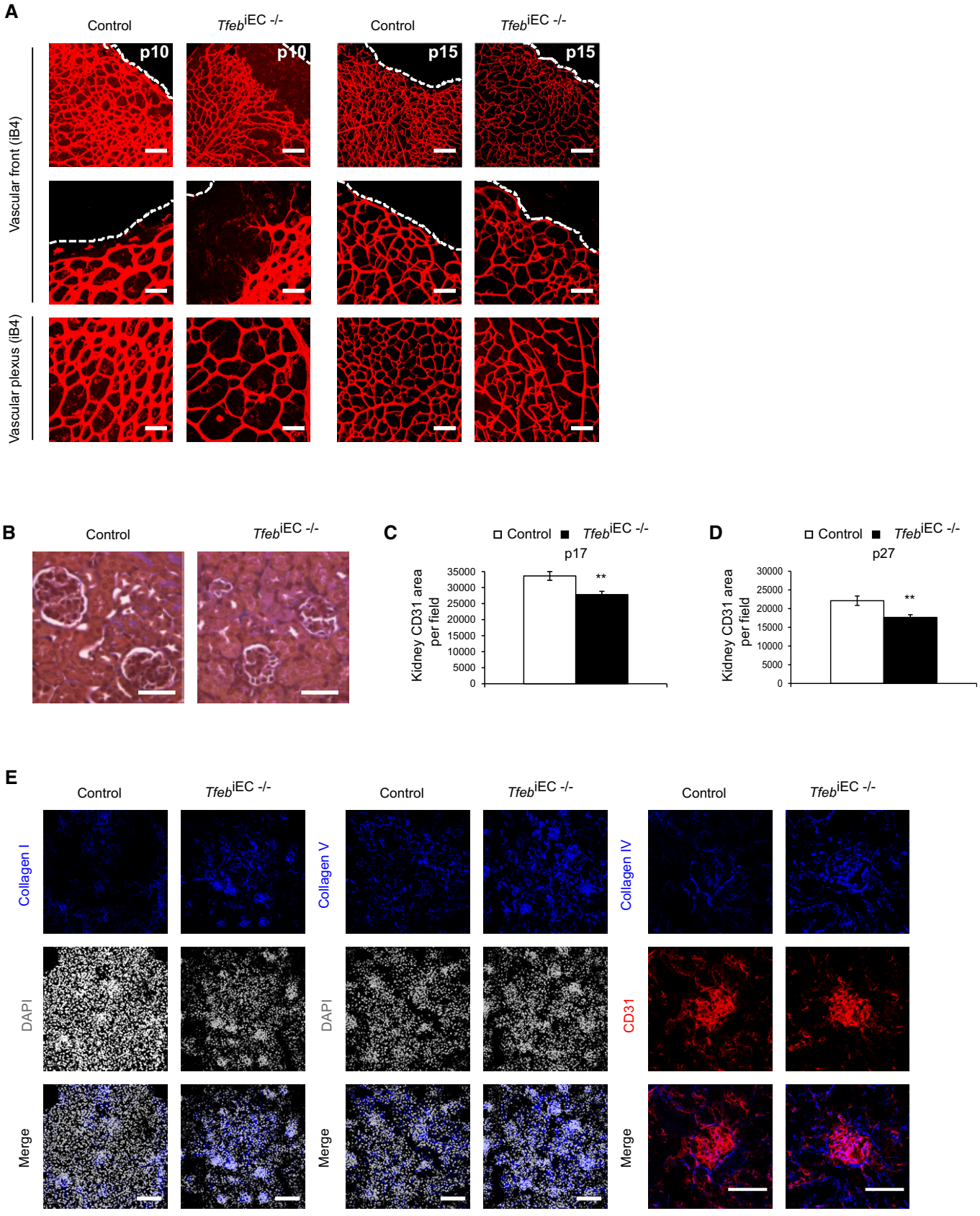
A
Control
Tfeb iEC -/-
Control
Tfeb iEC -/-
p10
p10
p15
p15
Vascular front (iB4)
Vascular plexus (iB4)
B
Control
Tfeb iEC -/-
C
Control
Tfeb iEC -/-
p17
Kidney CD31 area per field
35000
30000
25000
20000
15000
10000
5000
0
**
D
Control
Tfeb iEC -/-
p27
Kidney CD31 area per field
30000
25000
20000
15000
10000
5000
0
**
E
Control
Tfeb iEC -/-
Control
Tfeb iEC -/-
Control
Tfeb iEC -/-
Collagen I
Collagen V
Collagen IV
DAPI
DAPI
CD31
Merge
Merge
Merge

Figure EV3.

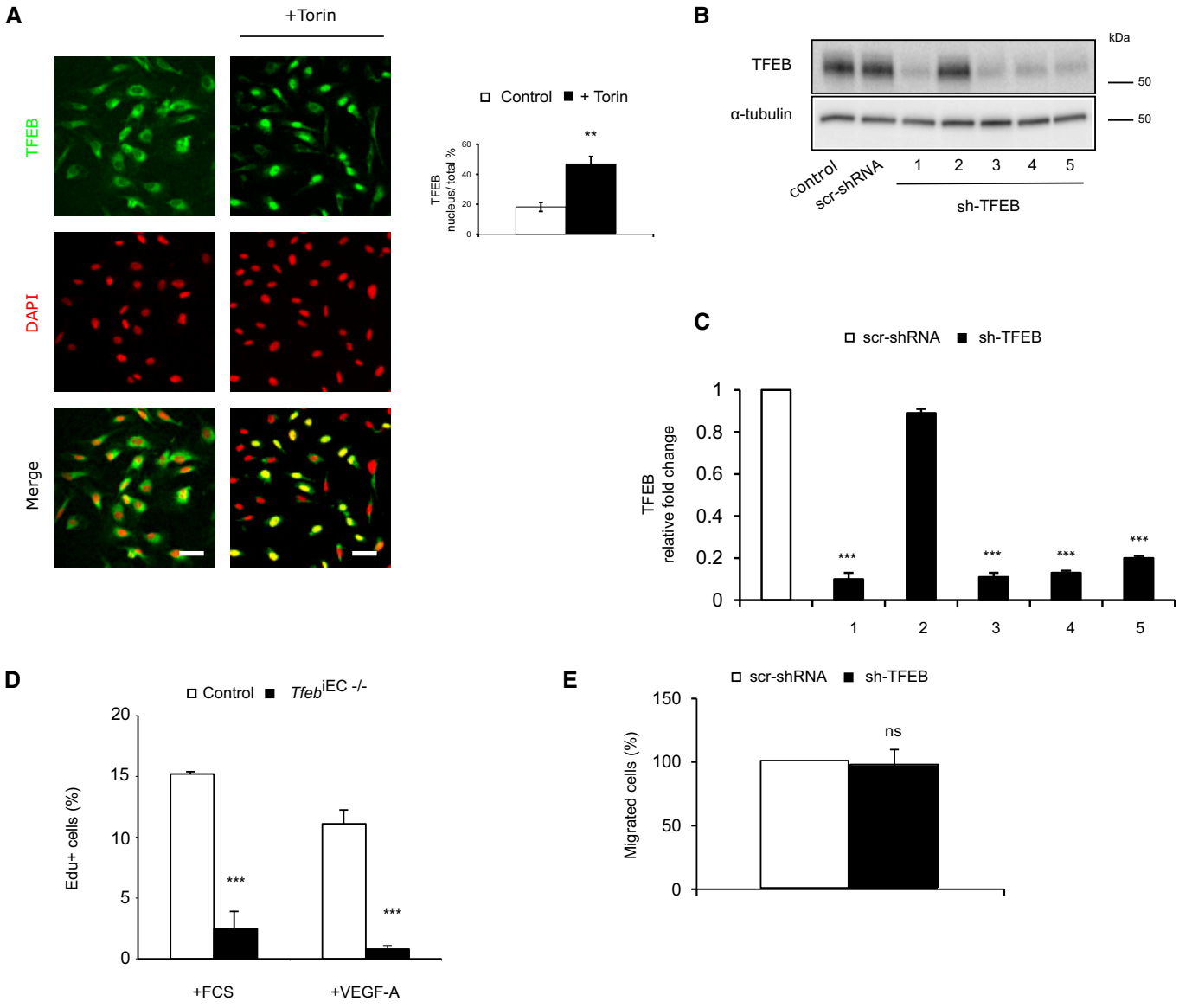

Figure EV4. TFEB expression and regulation in human ECs. Additional effects of *Tfeb* deletion on human ECs.

A mTOR inhibition activates TFEB nuclear translocation. Representative images of human ECs under basal conditions or after Torin stimulation (100 nM, 1 h) stained with anti-TFEB Ab and DAPI (scale bars: 20 μm). Bar graphs indicate the percentage of TFEB positive nuclei versus total nuclei after Torin challenge (n = 3, mean ± SEM; $^{**}P < 0.001$ versus control cells by Student's t-test).

B, C Characterization of TFEB shRNA (n = 3). (B) Western blot of TFEB in human ECs carrying five different commercial sh-TFEB RNAs (1-5) or the appropriate control (scr-shRNA) transduced by pLKO lentivirus vector. (C) *TFEB* mRNA expression analyzed by qPCR in ECs carrying the different TFEB shRNAs (1-5). Data are expressed as relative fold-change compared with scr-shRNA after normalization to the housekeeping gene TBP (n = 3, mean ± SEM; $^{***}P < 0.0001$ by Student's t-test).

D *TFEB* silencing reduced murine EC proliferation. Representative graph of lung ECs isolated from control and $Tfeb^{iEC-/-}$ mice ECs treated for 24 h with FCS (20%) or VEGF-A (30 ng/ml). DNA incorporation of EdU was detected by flow cytometry. The percentage of proliferating cells is indicated (n = 4, mean ± SEM; $^{***}P < 0.0001$ versus ECs derived from control mice by Student's t-test).

E *TFEB* silencing does not affect human EC migration. Bar graph indicates the percentage of migrated sh-TFEB and scr-shRNA ECs stimulated with VEGF-A (30 ng/ml, 5 h; n = 6, mean ± SEM, P = ns versus scr-shRNA by Student's t-test).

Source data are available online for this figure.

Figure EV5. TFEB gene regulation in human ECs.

A Volcano plots of human gene expression showing fold-change and *P*-value data comparing human sh-TFEB and scr-shRNA ECs. Red: up-regulated genes; green: down-regulated genes.

B Characterization of TFEBS142A overexpression in human ECs. Representative images of human ECs transduced with pTRIPZ-TFEBS142A inducible lentivirus (scale bars: 20 μm) after transgene induction with doxycycline (0.5 μg/ml, 3 h; TFEBS142A) or not (control) and stained with anti-TFEB Ab and DAPI. Bar graph indicates the quantity of cytosolic and nuclear TFEB as ratio between TFEBS142A and control ECs (n = 10, mean ± SEM, $^{**}P < 0.0001$ and $^{***}P < 0.0001$ by Student's t-test).

C Representative genomic view of the TFEB ChIP-seq analysis. The TFEB ChIP-seq plot shows distinct binding peaks with respect to the IgG ChIP-seq.

D Comparison of the TFEB-bound genomic regions with respect to the other indicated ChIP-seq regions taken from the literature. TFEB correlates with open chromatin (DNAse) and with transcription factors known to be associated with active gene promoters (FOS, JUN, RNA PolII, MYC).

E Enrichment of the E-box DNA-binding sequence of TFEB (CACGTG) on 70.9% of TFEB target genes in human ECs.

F Comparison of expression values in human ECs between TFEB-bound and unbound genes. Box plots are median-centered. The end of the box shows the upper and lower quartiles. The whiskers line shows the highest and lowest value excluding outliers.

G DNA methylation analysis of the TFEB-bound regions in human ECs using 450K Illumina microarray data from the literature (methylation status of 6,461 CpG has been analyzed).

H Genomic localization of TFEB-bound regions in human ECs.

I GSEA analysis of TFEB-bound genes comparing human sh-TFEB and scr-shRNA ECs microarray data. Enrichment plot shows modulated TFEB-bound genes.

J *TFEB* overexpression increased EC proliferation. Representative graph of control and TFEBS142A ECs treated for 24 h with FCS (20%). DNA incorporation of EdU was detected by flow cytometry. The percentage of proliferating cells is indicated (n = 4, mean ± SEM; $^{*}P < 0.01$ versus control ECs by Student's t-test).

K, L (K) qPCR and (L) immunoblots showing modulation of *CDK4* after TFEB overexpression in ECs. (K) Data are expressed as relative fold-change compared with the expression in control cells after normalization to the housekeeping gene TBP (n = 3, mean ± SEM; $^{***}P < 0.0001$ by Student's t-test). (L) Immunoblots of total lysates from control and TFEBS142A ECs probed with specific Abs. The bar graph shows the densitometric analysis expressed as % of CDK4 in TFEBS142A versus control ECs after the normalization with α-tubulin (n = 3, mean ± SEM; $^{***}P < 0.0001$ versus scr-shRNA by Student's t-test).

Source data are available online for this figure.

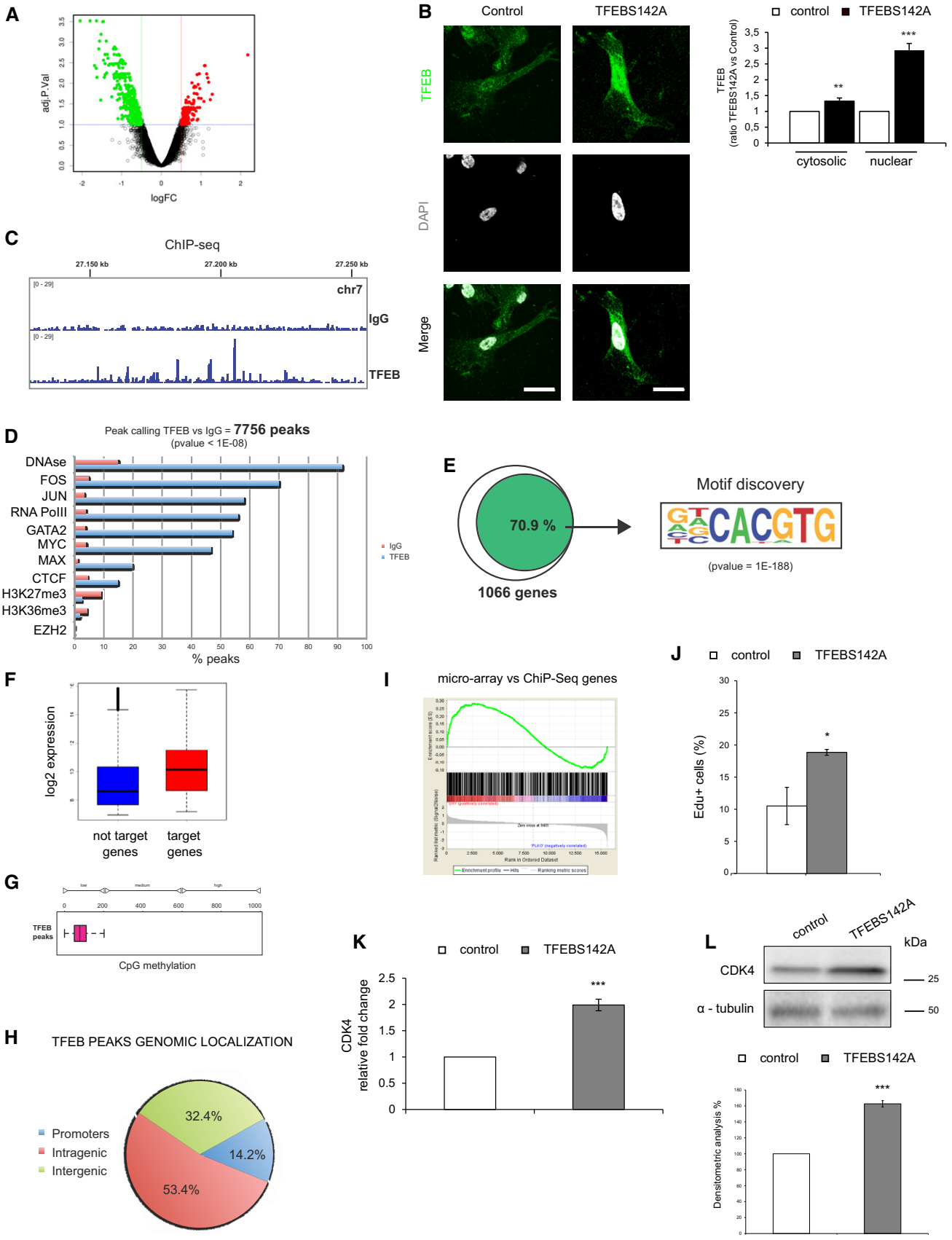

Figure EV5.